

Measurement of QED Structure Functions of the Photon using Azimuthal Correlations at LEP

The OPAL Collaboration

Abstract

We have studied azimuthal correlations in singly-tagged $e^+e^- \rightarrow e^+e^-\mu^+\mu^-$ events at an average Q^2 of 5.2 GeV^2 . The data were taken with the OPAL detector at LEP at e^+e^- centre-of-mass energies close to the Z^0 mass, with an integrated luminosity of approximately 100 pb^{-1} . The azimuthal correlations are used to extract the ratio F_B^γ/F_2^γ of the QED structure functions $F_B^\gamma(x, Q^2)$ and $F_2^\gamma(x, Q^2)$ of the photon. In leading order and neglecting the muon mass F_B^γ is expected to be identical to the longitudinal structure function F_L^γ . The measurement of F_B^γ/F_2^γ is found to be significantly different from zero and to be consistent with the QED prediction.

(Submitted to Zeit. f. Phys.)

The OPAL Collaboration

K. Ackerstaff⁸, G. Alexander²³, J. Allison¹⁶, N. Altekamp⁵, K. Ametewee²⁵, K.J. Anderson⁹, S. Anderson¹², S. Arcelli², S. Asai²⁴, D. Axen²⁹, G. Azuelos^{18,a}, A.H. Ball¹⁷, E. Barberio⁸, R.J. Barlow¹⁶, R. Bartoldus³, J.R. Batley⁵, J. Bechtluft¹⁴, C. Beeston¹⁶, T. Behnke⁸, A.N. Bell¹, K.W. Bell²⁰, G. Bella²³, S. Bentvelsen⁸, P. Berlich¹⁰, S. Bethke¹⁴, O. Biebel¹⁴, V. Blobel²⁷, I.J. Bloodworth¹, J.E. Bloomer¹, M. Bobinski¹⁰, P. Bock¹¹, H.M. Bosch¹¹, M. Boutemour³⁴, B.T. Bouwens¹², S. Braibant¹², R.M. Brown²⁰, H.J. Burckhart⁸, C. Burgard⁸, R. Bürgin¹⁰, P. Capiluppi², R.K. Carnegie⁶, A.A. Carter¹³, J.R. Carter⁵, C.Y. Chang¹⁷, D.G. Charlton^{1,b}, D. Chrisman⁴, P.E.L. Clarke¹⁵, I. Cohen²³, J.E. Conboy¹⁵, O.C. Cooke¹⁶, M. Cuffiani², S. Dado²², C. Dallapiccola¹⁷, G.M. Dallavalle², S. De Jong¹², L.A. del Pozo⁸, K. Desch³, M.S. Dixit⁷, E. do Couto e Silva¹², M. Doucet¹⁸, E. Duchovni²⁶, G. Duckeck³⁴, I.P. Duerdoth¹⁶, J.E.G. Edwards¹⁶, P.G. Estabrooks⁶, H.G. Evans⁹, M. Evans¹³, F. Fabbri², P. Fath¹¹, F. Fiedler²⁷, M. Fierro², H.M. Fischer³, R. Folman²⁶, D.G. Fong¹⁷, M. Foucher¹⁷, A. Fürtjes⁸, P. Gagnon⁷, A. Gaidot²¹, J.W. Gary⁴, J. Gascon¹⁸, S.M. Gascon-Shotkin¹⁷, N.I. Geddes²⁰, C. Geich-Gimbel³, F.X. Gentit²¹, T. Gerasis²⁰, G. Giacomelli², P. Giacomelli⁴, R. Giacomelli², V. Gibson⁵, W.R. Gibson¹³, D.M. Gingrich^{30,a}, D. Glenzinski⁹, J. Goldberg²², M.J. Goodrick⁵, W. Gorn⁴, C. Grandi², E. Gross²⁶, J. Grunhaus²³, M. Gruwé⁸, C. Hajdu³², G.G. Hanson¹², M. Hansroul⁸, M. Hapke¹³, C.K. Hargrove⁷, P.A. Hart⁹, C. Hartmann³, M. Hauschild⁸, C.M. Hawkes⁵, R. Hawkings⁸, R.J. Hemingway⁶, M. Herndon¹⁷, G. Herten¹⁰, R.D. Heuer⁸, M.D. Hildreth⁸, J.C. Hill⁵, S.J. Hillier¹, T. Hilse¹⁰, P.R. Hobson²⁵, R.J. Homer¹, A.K. Honma^{28,a}, D. Horváth^{32,c}, R. Howard²⁹, R.E. Hughes-Jones¹⁶, D.E. Hutchcroft⁵, P. Igo-Kemenes¹¹, D.C. Imrie²⁵, M.R. Ingram¹⁶, K. Ishii²⁴, A. Jawahery¹⁷, P.W. Jeffreys²⁰, H. Jeremie¹⁸, M. Jimack¹, A. Joly¹⁸, C.R. Jones⁵, G. Jones¹⁶, M. Jones⁶, R.W.L. Jones⁸, U. Jost¹¹, P. Jovanovic¹, T.R. Junk⁸, D. Karlen⁶, K. Kawagoe²⁴, T. Kawamoto²⁴, R.K. Keeler²⁸, R.G. Kellogg¹⁷, B.W. Kennedy²⁰, B.J. King⁸, J. Kirk²⁹, S. Kluth⁸, T. Kobayashi²⁴, M. Kobel¹⁰, D.S. Koetke⁶, T.P. Kokott³, M. Kolrep¹⁰, S. Komamiya²⁴, T. Kress¹¹, P. Krieger⁶, J. von Krogh¹¹, P. Kyberd¹³, G.D. Lafferty¹⁶, H. Lafoux²¹, R. Lahmann¹⁷, W.P. Lai¹⁹, D. Lanske¹⁴, J. Lauber¹⁵, S.R. Lautenschlager³¹, J.G. Layter⁴, D. Lazic²², A.M. Lee³¹, E. Lefebvre¹⁸, D. Lellouch²⁶, J. Letts², L. Levinson²⁶, C. Lewis¹⁵, S.L. Lloyd¹³, F.K. Loebinger¹⁶, G.D. Long¹⁷, M.J. Losty⁷, J. Ludwig¹⁰, A. Malik²¹, M. Mannelli⁸, S. Marcellini², C. Markus³, A.J. Martin¹³, J.P. Martin¹⁸, G. Martinez¹⁷, T. Mashimo²⁴, W. Matthews²⁵, P. Mättig³, W.J. McDonald³⁰, J. McKenna²⁹, E.A. Mckigney¹⁵, T.J. McMahon¹, A.I. McNab¹³, R.A. McPherson⁸, F. Meijers⁸, S. Menke³, F.S. Merritt⁹, H. Mes⁷, J. Meyer²⁷, A. Michelini², G. Mikenberg²⁶, D.J. Miller¹⁵, R. Mir²⁶, W. Mohr¹⁰, A. Montanari², T. Mori²⁴, M. Morii²⁴, U. Müller³, K. Nagai²⁶, I. Nakamura²⁴, H.A. Neal⁸, B. Nellen³, B. Nijjar¹⁶, R. Nisius⁸, S.W. O'Neale¹, F.G. Oakham⁷, F. Odorici², H.O. Ogren¹², N.J. Oldershaw¹⁶, T. Omori²⁴, M.J. Oreglia⁹, S. Orito²⁴, J. Pálincás^{33,d}, G. Pásztor³², J.R. Pater¹⁶, G.N. Patrick²⁰, J. Patt¹⁰, M.J. Pearce¹, S. Petzold²⁷, P. Pfeifenschneider¹⁴, J.E. Pilcher⁹, J. Pinfold³⁰, D.E. Plane⁸, P. Poffenberger²⁸, B. Poli², A. Posthaus³, H. Przystecznik³⁰, D.L. Rees¹, D. Rigby¹, S. Robertson²⁸, S.A. Robins¹³, N. Rodning³⁰, J.M. Roney²⁸, A. Rooke¹⁵, E. Ros⁸, A.M. Rossi², M. Rosvick²⁸, P. Routenburg³⁰, Y. Rozen²², K. Runge¹⁰, O. Runolfsson⁸, U. Ruppel¹⁴, D.R. Rust¹², R. Rylko²⁵, K. Sachs¹⁰, E.K.G. Sarkisyan²³, M. Sasaki²⁴, C. Sbarra², A.D. Schaile³⁴, O. Schaile³⁴, F. Scharf³, P. Scharff-Hansen⁸, P. Schenk²⁷, B. Schmitt⁸, S. Schmitt¹¹, M. Schröder⁸, H.C. Schultz-Coulon¹⁰, M. Schulz⁸, M. Schumacher³, P. Schütz³, W.G. Scott²⁰, T.G. Shears¹⁶, B.C. Shen⁴, C.H. Shepherd-Themistocleous⁸, P. Sherwood¹⁵, G.P. Siroli², A. Sittler²⁷, A. Skillman¹⁵, A. Skuja¹⁷, A.M. Smith⁸, T.J. Smith²⁸, G.A. Snow¹⁷, R. Sobie²⁸,

S. Söldner-Rembold¹⁰, R.W. Springer³⁰, M. Sproston²⁰, A. Stahl³, M. Steiert¹¹, K. Stephens¹⁶,
J. Steuerer²⁷, B. Stockhausen³, D. Strom¹⁹, F. Strumia⁸, P. Szymanski²⁰, R. Tafirout¹⁸,
S.D. Talbot¹, S. Tanaka²⁴, P. Taras¹⁸, S. Tarem²², M. Thiergen¹⁰, M.A. Thomson⁸, E. von
Törne³, S. Towers⁶, I. Trigger¹⁸, T. Tsukamoto²⁴, E. Tsur²³, A.S. Turcot⁹,
M.F. Turner-Watson⁸, P. Utzat¹¹, R. Van Kooten¹², G. Vasseur²¹, M. Verzocchi¹⁰, P. Vikas¹⁸,
M. Vinciter²⁸, E.H. Vokurka¹⁶, F. Wäckerle¹⁰, A. Wagner²⁷, C.P. Ward⁵, D.R. Ward⁵,
J.J. Ward¹⁵, P.M. Watkins¹, A.T. Watson¹, N.K. Watson⁷, P.S. Wells⁸, N. Vermes³,
J.S. White²⁸, B. Wilkens¹⁰, G.W. Wilson²⁷, J.A. Wilson¹, G. Wolf²⁶, S. Wotton⁵, T.R. Wyatt¹⁶,
S. Yamashita²⁴, G. Yekutieli²⁶, V. Zacek¹⁸,

¹School of Physics and Space Research, University of Birmingham, Birmingham B15 2TT, UK

²Dipartimento di Fisica dell' Università di Bologna and INFN, I-40126 Bologna, Italy

³Physikalisches Institut, Universität Bonn, D-53115 Bonn, Germany

⁴Department of Physics, University of California, Riverside CA 92521, USA

⁵Cavendish Laboratory, Cambridge CB3 0HE, UK

⁶Ottawa-Carleton Institute for Physics, Department of Physics, Carleton University, Ottawa, Ontario K1S 5B6, Canada

⁷Centre for Research in Particle Physics, Carleton University, Ottawa, Ontario K1S 5B6, Canada

⁸CERN, European Organisation for Particle Physics, CH-1211 Geneva 23, Switzerland

⁹Enrico Fermi Institute and Department of Physics, University of Chicago, Chicago IL 60637, USA

¹⁰Fakultät für Physik, Albert Ludwigs Universität, D-79104 Freiburg, Germany

¹¹Physikalisches Institut, Universität Heidelberg, D-69120 Heidelberg, Germany

¹²Indiana University, Department of Physics, Swain Hall West 117, Bloomington IN 47405, USA

¹³Queen Mary and Westfield College, University of London, London E1 4NS, UK

¹⁴Technische Hochschule Aachen, III Physikalisches Institut, Sommerfeldstrasse 26-28, D-52056 Aachen, Germany

¹⁵University College London, London WC1E 6BT, UK

¹⁶Department of Physics, Schuster Laboratory, The University, Manchester M13 9PL, UK

¹⁷Department of Physics, University of Maryland, College Park, MD 20742, USA

¹⁸Laboratoire de Physique Nucléaire, Université de Montréal, Montréal, Quebec H3C 3J7, Canada

¹⁹University of Oregon, Department of Physics, Eugene OR 97403, USA

²⁰Rutherford Appleton Laboratory, Chilton, Didcot, Oxfordshire OX11 0QX, UK

²¹CEA, DAPNIA/SPP, CE-Saclay, F-91191 Gif-sur-Yvette, France

²²Department of Physics, Technion-Israel Institute of Technology, Haifa 32000, Israel

²³Department of Physics and Astronomy, Tel Aviv University, Tel Aviv 69978, Israel

²⁴International Centre for Elementary Particle Physics and Department of Physics, University of Tokyo, Tokyo 113, and Kobe University, Kobe 657, Japan

²⁵Brunel University, Uxbridge, Middlesex UB8 3PH, UK

²⁶Particle Physics Department, Weizmann Institute of Science, Rehovot 76100, Israel

²⁷Universität Hamburg/DESY, II Institut für Experimental Physik, Notkestrasse 85, D-22607 Hamburg, Germany

²⁸University of Victoria, Department of Physics, P O Box 3055, Victoria BC V8W 3P6, Canada

²⁹University of British Columbia, Department of Physics, Vancouver BC V6T 1Z1, Canada

³⁰University of Alberta, Department of Physics, Edmonton AB T6G 2J1, Canada

³¹Duke University, Dept of Physics, Durham, NC 27708-0305, USA

³²Research Institute for Particle and Nuclear Physics, H-1525 Budapest, P O Box 49, Hungary

³³Institute of Nuclear Research, H-4001 Debrecen, P O Box 51, Hungary

³⁴Ludwigs-Maximilians-Universität München, Sektion Physik, Am Coulombwall 1, D-85748 Garching, Germany

^a and at TRIUMF, Vancouver, Canada V6T 2A3

^b and Royal Society University Research Fellow

^c and Institute of Nuclear Research, Debrecen, Hungary

^d and Department of Experimental Physics, Lajos Kossuth University, Debrecen, Hungary

1 Introduction

The study of two-photon events in e^+e^- colliders provides a good way to test Quantum Electrodynamics (QED). As in the case of ep collisions, which permit us to probe the structure of the proton, electron-photon collisions enable us to probe the structure of the photon. Two-photon events are studied through the reaction $e^+e^- \rightarrow e^+e^-X$. Most of the electrons¹ in this reaction are scattered at very low angles and are lost along the beam pipe. To study the structure of the photon, at least one of the electrons must be observed in the detector. The $e\gamma$ cross-section is given [1] by:

$$\frac{d\sigma(e\gamma \rightarrow eX)}{dx dQ^2} = \frac{2\pi\alpha^2}{xQ^4} \left[(1 + (1-y)^2) F_2^\gamma(x, Q^2) - y^2 F_L^\gamma(x, Q^2) \right]. \quad (1)$$

It is related to the e^+e^- cross-section by the Weizsäcker-Williams approximation [2] for the flux of quasi-real photons. The kinematics are defined by the Bjorken variable x , the dimensionless variable y and the four-momentum squared Q^2 of the virtual photon emitted by the tagged electron (these parameters are discussed in section 2). The functions F_2^γ and F_L^γ are called structure functions and α is the QED coupling constant. The structure functions F_2^γ for leptonic final states [3] (described by QED) and for hadronic final-states [4] (described by QCD) have already been measured by OPAL. The longitudinal structure function F_L^γ is very difficult to measure at LEP [5] because its contribution is small and is weighted by the factor y^2 . The energy of the tagged electron is usually required to be larger than half the beam energy to reduce backgrounds, which gives values of y much less than unity. As an alternative to the direct measurement of F_L^γ , it has been pointed out [6-11] that there are azimuthal correlations in the final-state particles from two-photon collisions which are sensitive to additional structure functions. The longitudinal structure function F_L^γ has been shown to be equal to the structure function F_B^γ in leading order and for massless muons, although coming from different helicity states of the photons. Azimuthal correlations can thus supplement the direct measurement of structure functions from total cross-sections. In this paper we publish the first measurement of F_B^γ through azimuthal correlations in muonic two-photon events. The data sample consists of all the OPAL data taken at centre-of-mass energies on and near the mass of the Z^0 since the upgrade of the forward detectors, amounting to approximately 100 pb^{-1} .

2 Kinematics of two-photon events

We are interested in muonic two-photon events (see figure 1) where one of the scattered electrons (the tag) is detected at low angle relative to the beam axis in the range of $0.026 < \sin \theta_{\text{tag}} < 0.120$, while the other (the anti-tag) is lost in the beam pipe. The photon associated with the anti-tagged electron is assumed to be close to real and directed along the z axis. The variables which describe these events are defined in the following way [1]:

$$Q^2 = -q^2 \simeq 2E_b E_{\text{tag}} (1 - \cos \theta_{\text{tag}}), \quad (2)$$

$$x = \frac{-q^2}{W^2 - q^2 - p^2} \simeq \frac{Q^2}{W^2 + Q^2}, \quad (3)$$

¹Positrons are also referred to as electrons.

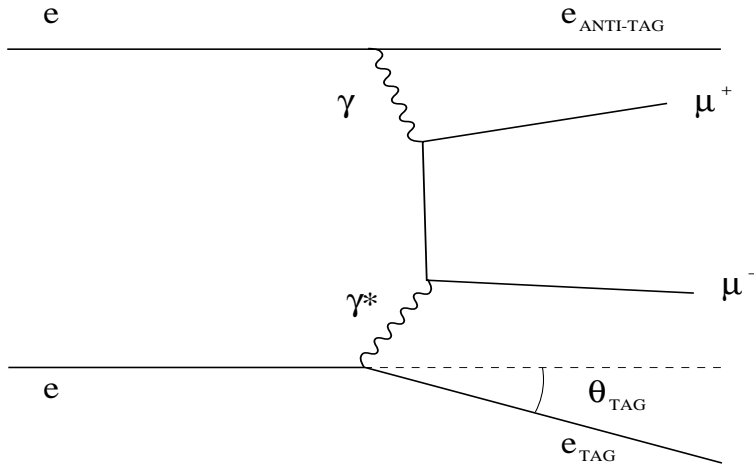


Figure 1: Diagram of an $e^+e^- \rightarrow e^+e^-\mu^+\mu^-$ event.

$$y = \frac{q \cdot p}{q \cdot k} \simeq 1 - \frac{E_{\text{tag}}}{E_b} \cos^2 \frac{\theta_{\text{tag}}}{2}, \quad (4)$$

where q is the momentum of the virtual photon, p is the momentum of the quasi-real photon, k is the initial momentum of the electron associated with the tag, W^2 is the squared invariant mass of the $\mu^+\mu^-$ system, E_{tag} is the energy of the tagged electron, θ_{tag} is its polar angle with respect to the beam direction and E_b is the beam energy. The main variable in this analysis is the azimuthal angle χ (figure 2), defined in the $\gamma^*\gamma$ centre-of-mass frame as the angle between the planes formed by the $\gamma^*\gamma$ axis and the directions of the μ^- and e_{tag}^- , respectively (for e^- tags) or the angle between the planes formed by the $\gamma^*\gamma$ axis and the directions of the μ^+ and e_{tag}^+ , respectively (for e^+ tags). We also define $\eta = \cos\theta^*$, where θ^* is the angle between the μ^- (μ^+) and the photon axis in the $\gamma^*\gamma$ centre-of-mass. The cross-section of the process which

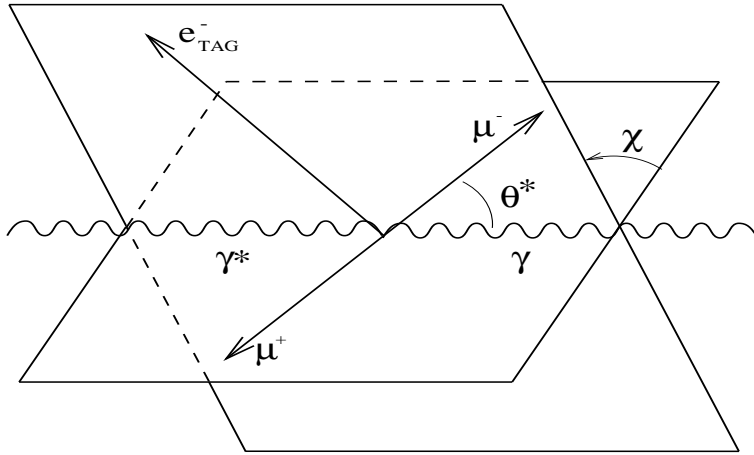


Figure 2: Illustration of the azimuthal angle.

interests us may be written in the following way (see for example [11]):

$$\frac{d\sigma(e\gamma \rightarrow e\mu^+\mu^-)}{dx dy d\eta d\chi/4\pi} = \frac{2\pi\alpha^2}{Q^2} \left(\frac{1 + (1-y)^2}{xy} \right) \times \left[(2x\tilde{F}_T^\gamma + \epsilon(y)\tilde{F}_L^\gamma) - \rho(y)\tilde{F}_A^\gamma \cos\chi + \frac{1}{2}\epsilon(y)\tilde{F}_B^\gamma \cos 2\chi \right], \quad (5)$$

with

$$\begin{aligned}\epsilon(y) &= 2\frac{1-y}{1+(1-y)^2} \simeq 1 \quad (\text{for small } y), \\ \rho(y) &= \sqrt{\epsilon(1+\epsilon)/2} \simeq 1 \quad (\text{for small } y),\end{aligned}\tag{6}$$

where \tilde{F}_T^γ , \tilde{F}_A^γ , \tilde{F}_B^γ and \tilde{F}_L^γ are differential structure functions. The functions $\epsilon(y)$ and $\rho(y)$ are approximately equal to unity for small y . The dependence of the QED cross-section on the azimuthal angle χ is explicit in equation 5 and the QED differential structure functions do not depend on χ . The conventional structure functions F_i^γ can be recovered by integration over η and χ :

$$F_{T,A,B,L}^\gamma = \int_{-1}^1 \int_0^{2\pi} \frac{d\eta d\chi}{4\pi} \tilde{F}_{T,A,B,L}^\gamma.\tag{7}$$

We also have the following definition [1]:

$$F_2^\gamma = 2xF_T^\gamma + F_L^\gamma,\tag{8}$$

with the leading order identity

$$F_B^\gamma(x) = F_L^\gamma(x) = \frac{4\alpha}{\pi} x^2(1-x),\tag{9}$$

neglecting the mass dependent terms. We also have [12]

$$F_B^\gamma(x, Q^2) = \frac{4\alpha}{\pi} x^2 \left[(1-x) \left(1 - \frac{2m_\mu^2}{Q^2}\right) \sqrt{1 - \frac{4m_\mu^2}{W^2}} - \frac{2m_\mu^2}{W^2 + Q^2} \log \frac{1 + \sqrt{1 - \frac{4m_\mu^2}{W^2}}}{1 - \sqrt{1 - \frac{4m_\mu^2}{W^2}}} \frac{W^2 - Q^2 - 2m_\mu^2}{Q^2} \right],\tag{10}$$

where the mass dependent terms are included and m_μ is the mass of the muon. The structure functions F_i^γ are combinations of transition amplitudes for different helicity states of the photons. The structure function F_B^γ is related to the interference term between two transverse helicity states of the photons. It is identical to F_L^γ , which is related to the longitudinal polarization of the virtual photon, in leading order and for massless muons. It is not known if this identity is still valid for higher orders. The first term of the cross-section (equation 5), independent of χ , has already been measured with OPAL [3] and is associated with F_2^γ . The study of azimuthal correlations gives some information about the structure functions F_A^γ and F_B^γ . The structure function F_A^γ will not be studied in this note. Its contribution is zero when integrated over η (see for example in [11] that \tilde{F}_A^γ is antisymmetric in η). Assuming that \tilde{F}_B^γ is independent of χ [11], the cross-section integrated over η may be re-written:

$$\frac{d\sigma(e\gamma \rightarrow e\mu^+\mu^-)}{dx dy d\chi/2\pi} \simeq \frac{2\pi\alpha^2}{Q^2} \left(\frac{1+(1-y)^2}{xy} \right) \times F_2^\gamma \left(1 + \frac{1}{2}\epsilon(F_B^\gamma/F_2^\gamma) \cos 2\chi \right).\tag{11}$$

3 The OPAL Detector

The OPAL detector is described elsewhere [13] and only the constituents which are relevant to this analysis are presented in this section. The OPAL detector consists of a tracking system inside a uniform magnetic field of 0.435 T directed along the beam axis. The coil providing the

magnetic field is surrounded by electromagnetic calorimeters (ECAL), hadronic calorimeters (HCAL) and muon chambers. Each endcap has a similar coverage of calorimeters.

The primary charged track detection is made by a large jet chamber immersed in the magnetic field. A charged track may give a maximum of 159 sense wire hits in the polar angle region, relative to the beam axis, above 0.754 rad, and a maximum between 20 and 159 in the polar angle region between 0.274 rad and 0.754 rad. The jet chamber is surrounded by drift chambers which measure the coordinates of charged particles in the direction parallel to the beam axis. Also important in this analysis are the forward detector (FD) and the silicon-tungsten calorimeter (SiW). They both cover small angles relative to the beam direction. The forward detector consists of 24 radiation lengths of lead-scintillator calorimeters having an energy resolution of about $18\%/\sqrt{E(\text{GeV})}$. The silicon-tungsten calorimeter consists of 18 layers of tungsten sandwiched between 19 layers of silicon detectors, amounting to 22 radiation lengths. Its energy resolution is about $25\%/\sqrt{E(\text{GeV})}$. The silicon-tungsten calorimeter is used to detect particles in the polar angle region between 25 and 60 mrad and the forward detector is used for the higher range from 60 mrad to 120 mrad.

The coordinates in the OPAL detector are defined such that the z axis is given by the direction of the electron beam, the x axis is directed towards the centre of the LEP ring and the y axis is directed upwards.

4 Monte Carlo simulation

The Vermaseren 1.01 [14] generator was used to simulate a Monte Carlo sample of $e^+e^- \rightarrow e^+e^-\mu^+\mu^-$ events corresponding to an integrated luminosity of 340 pb^{-1} . These events were generated with $E_b = 46.0 \text{ GeV}$ and $W_{\text{min}} = 2m_\mu$. A selection was made at the generator level to keep only events with one electron in FD or SiW ($0.024 < \sin \theta_{\text{tag}} < 0.140$). Since a significant fraction of events have muons with a low polar angle with respect to the beam axis, where they are not detectable, the events with one or both muons having $|\cos \theta_\mu| > 0.975$ were rejected. The cut $E_{\text{tag}} > 20 \text{ GeV}$ was also applied. The events were processed by the full simulation program of the OPAL detector [15].

5 Event selection

Events with one tagged electron and two charged tracks, of which at least one was identified as a muon, were selected. The requirements for the tagged electron are:

1. E_{tag} greater than half the energy of the beam, the energy being completely contained in either FD or SiW,
2. an angle θ_{tag} in the range $0.026 < \sin \theta_{\text{tag}} < 0.120$.

The selected angular range of the tagged electron corresponds to a range in Q^2 of $0.85 < Q^2 < 31 \text{ GeV}^2$. A charged track was accepted if it satisfied the following criteria:

1. at least 20 hits in the jet chamber,
2. a distance of closest approach, d_0 , to the nominal beam axis of less than 1.0 cm, and $|z| < 20$ cm at the point of closest approach,
3. momentum between 0.3 and 20 GeV/ c ,
4. transverse momentum relative to the beam direction greater than 0.1 GeV/ c .

No restriction on the polar angle of the muons was made. The angle of the muons is thus restricted by the acceptance of the OPAL detector, which extends to $|\cos \theta_\mu| = 0.962$. A track was identified as a muon if it met the following criteria:

1. momentum greater than 1 GeV/ c ,
2. energy deposited in the ECAL less than 1.5 GeV,
3. either a good muon signal in the HCAL or in the muon chambers, as described in [3].

In order to have a more precise energy measurement for the tag, this energy was evaluated using energy and longitudinal momentum conservation in the event. Since the precision is greater for the angle of the tag than for its energy, the following relation was used:

$$E_{\text{tag}} = \frac{P_{\mu^+\mu^-} \cos \theta_{\mu^+\mu^-} + (2E_b - E_{\mu^+\mu^-}) \cos \theta_{\text{anti-tag}}}{\cos \theta_{\text{anti-tag}} - \cos \theta_{\text{tag}}}, \quad (12)$$

where the lepton masses were neglected. $E_{\mu^+\mu^-}$ is the energy of the muon pair system, $P_{\mu^+\mu^-}$ its momentum and $\theta_{\mu^+\mu^-}$ its polar angle. $\theta_{\text{anti-tag}}$ is the polar angle of the anti-tag, which was assumed to be 0 or π , depending on whether the tag was in the $-z$ or $+z$ direction, respectively. Using this method, the resolution on E_{tag} was improved from 2 GeV to about 0.5 GeV. Figure 3 shows $E_{\text{tag}} - E_{\text{tag,MC}}$, where $E_{\text{tag,MC}}$ is the true tagged electron energy, versus the angle of the tag for both the energy measured by the calorimeters and the one obtained using equation 12.

Figure 4 shows the distributions of E_{tag}/E_b , $\sin \theta_{\text{tag}}$, η , W , y and x for the selected Monte Carlo events and OPAL data. The x distribution ranges between 0.001 and 0.997. The small discrepancies seen in the distributions are not important for the analysis. Their possible effect is taken into account when evaluating the systematic errors. The discrepancy between data and Monte Carlo at small $\sin \theta_{\text{tag}}$ is due to the detector simulation. This discrepancy has no influence on the measurement of the azimuthal correlations. It changes, however, the average Q^2 which is measured to be 5.21 ± 0.04 (statistical) GeV² in the data compared to 5.00 ± 0.02 (statistical) GeV² in the Monte Carlo. A total of 14878 events passed the selection criteria; 3712 of these had a tag in FD and 11166 had a tag in SiW.

6 Azimuthal angle distribution

In order to measure the azimuthal angle χ , one needs to boost the momentum of each particle to the $\gamma^*\gamma$ centre-of-mass system. This boost is found using the combined momentum of the

muons. The azimuthal angle χ is well measured. The resolution, of about 20 mrad, is nearly constant over the whole χ range. Figure 5 shows the azimuthal angle distributions for both the Monte Carlo sample and the data. These distributions do not exhibit directly the $\cos 2\chi$ dependence predicted by QED (eq. 11). This is due to the acceptance of the detector, mainly for the muons lost in the forward region, in the polar angle range between the acceptance limit of the central detector and the beam axis. In order to extract F_B^γ , one needs to correct the azimuthal angle distributions of figure 5 for this detector effect. A bin-by-bin correction in χ , for every range of x , was applied to the data distributions. The technique used consists of dividing each χ distribution for the data by the corresponding χ distribution for the Monte Carlo, which was weighted by $1/(1 + \frac{1}{2}\epsilon F_B^\gamma/F_2^\gamma \cos 2\chi)$, where the structure functions are the analytical QED structure functions. The weighted distribution is equivalent to that which would have been obtained had we generated a Monte Carlo with a flat azimuthal angle distribution. Once the azimuthal angle distributions were corrected, they were fitted to the following function:

$$F(\chi) = A(1 + B \cos 2\chi), \quad (13)$$

where A is a normalization factor and B gives the ratio of F_B^γ to F_2^γ (see equation 11). The fitted distributions are shown in figure 6.

7 Background and systematic errors

Various sources of backgrounds were considered. The principal source of contamination is expected to be muonic decays of tau pairs. The KORALZ generator [16] was used to estimate the contribution of $e^+e^- \rightarrow Z^0 \rightarrow \tau^+\tau^-$ events, the Vermaseren generator [14] was used to estimate the background from $e^+e^- \rightarrow e^+e^-\tau^+\tau^-$ events and the HERWIG generator [17] was used to estimate the background from hadronic two-photon events. The background from $\gamma^*\gamma \rightarrow \pi^+\pi^-$ was also considered and was estimated to be negligible [18]. The estimated backgrounds are shown in table 1.

The background, being very small (about 2.7%), was not subtracted from the signal. Its effect was included in the systematic error by fitting the azimuthal angle distribution of the simulation of the background to equation 13, and taking 2.7% of the resulting fitted value of B as the systematic uncertainty on the B values derived from the data sample.

Because of the role of the Monte Carlo in providing the correction to obtain the shape of the azimuthal angle distribution, the following tests were made to establish the reliability of the procedure. The systematic uncertainties are shown in table 2.

1. The resolution on x , Q^2 and χ :

The effects of the resolution on each of these three variables were included by varying the shape of the distribution of each variable in turn according to its resolution in the Monte Carlo (the average resolution was found to be about 5% for each variable). The average deviation of $\frac{1}{2}\epsilon F_B^\gamma/F_2^\gamma$ was taken as the systematic error. This variation was done by re-weighting the Monte Carlo events.

2. The resolution on η and y :

The variable η does not appear explicitly in the analysis. The theoretical structure

functions used in the correction are integrated over η , so that the correction assumes the QED η distribution. Figure 4(c) shows the measured η distribution compared to the QED prediction. To take into account the resolution on η , the shape of the Monte Carlo distribution was changed according to the η resolution (which was found to be about 5%). This was done by weighting each Monte Carlo event. The average deviation of $\frac{1}{2}\epsilon F_B^\gamma/F_2^\gamma$ was taken as the systematic error. The same technique was used to estimate the systematic error due to the resolution on y , which is about 9%.

3. Effects of the correction:

In order to estimate properly the error on the fitted parameter B , a Monte Carlo in which the ratio of F_B^γ to F_2^γ was varied was used to verify the sensitivity to F_B^γ . This test used the TWOGEN [19] generator, modified to produce different azimuthal angle distributions. Several Monte Carlo samples were generated with different ratios of F_B^γ to F_2^γ . Simple cuts were applied to the samples in order to reproduce the effects of the detector. The cuts are the following:

- (a) one electron (corresponding to the tag) with $\sin\theta_{\text{tag}} > 0.024$ and $E_{\text{tag}} > 20$ GeV,
- (b) the other electron with $\sin\theta_{\text{anti-tag}} < 0.027$,
- (c) the muons having $|\cos\theta_\mu| < 0.962$, the lower muon momentum above 0.3 GeV/ c and the higher above 1.0 GeV/ c .

The azimuthal angle distributions for each of these samples were corrected with an azimuthal angle distribution corresponding to a value of $F_B^\gamma = 0$. The sensitivity to F_B^γ was estimated by comparing the output ratio of the two structure functions to the input ratio. A one-to-one correspondence was found between the input and the output within 2% to 5%. To take this effect into account, the errors on the data points for the different bins of x were multiplied by factors varying between 1.02 and 1.05.

8 Results and conclusions

The value of $\frac{1}{2}\epsilon F_B^\gamma/F_2^\gamma$ for each x range is shown in figure 7 and compared to the QED prediction for $Q^2 = 5.2$ GeV² and $\epsilon = 1$. The values are plotted according to the prescription described in [20]. The four values of $\frac{1}{2}\epsilon F_B^\gamma/F_2^\gamma$ are given in table 2 with their statistical and systematic errors. The measured value of $\frac{1}{2}\epsilon F_B^\gamma/F_2^\gamma$ over the whole x range is $0.076 \pm 0.013 \pm 0.015$, close to the QED prediction of 0.083. The variation with x is consistent with QED ($\chi^2/\text{dof} = 0.94$) although it is also consistent with a constant F_B^γ/F_2^γ ($\chi^2/\text{dof} = 0.74$). The measured values are nonetheless significantly different from zero ($\chi^2/\text{dof} = 6.7$).

In summary, azimuthal correlations can supplement the direct measurement of structure functions from total cross-sections. We have made the first measurement of the size of the ratio of the structure functions F_B^γ and F_2^γ for muonic two-photon events, based on azimuthal correlations in data from the OPAL experiment at LEP. This structure function F_B^γ is identical to the structure function F_L^γ in leading order for massless muons. This identity enables us to infer information about the structure of the photon that we would have obtained had we measured F_L^γ , although these two structure functions come from different helicity states of the photons. A first attempt to measure the variation of F_B^γ/F_2^γ with the scaling variable x has also

been obtained, although there is as yet no sensitivity to distinguish that from an x -independent F_B^γ/F_2^γ .

Acknowledgements

We particularly wish to thank the SL Division for the efficient operation of the LEP accelerator and for their continuing close cooperation with our experimental group. We thank John H. Field and Mike Seymour for valuable discussions. In addition to the support staff at our own institutions we are pleased to acknowledge the

Department of Energy, USA,

National Science Foundation, USA,

Particle Physics and Astronomy Research Council, UK,

Natural Sciences and Engineering Research Council, Canada,

Israel Science Foundation, administered by the Israel Academy of Science and Humanities,

Minerva Gesellschaft,

Japanese Ministry of Education, Science and Culture (the Monbusho) and a grant under the Monbusho International Science Research Program,

German Israeli Bi-national Science Foundation (GIF),

Direction des Sciences de la Matière du Commissariat à l'Énergie Atomique, France,

Bundesministerium für Bildung, Wissenschaft, Forschung und Technologie, Germany,

National Research Council of Canada,

Hungarian Foundation for Scientific Research, OTKA T-016660, and OTKA F-015089.

References

- [1] V. M. Budnev et al., *Phys. Rep.* **15**, 181 (1974).
- [2] C. F. von Weizsäcker, *Zeit. f. Phys.* **88**, 612 (1934);
E. J. Williams, *Phys. Rev.* **45**, 729 (1934).
- [3] OPAL Collaboration, R. Akers et al., *Zeit. f. Phys.* **C60**, 593 (1993).
- [4] OPAL Collaboration, R. Akers et al., *Zeit. f. Phys.* **C61**, 199 (1994).
- [5] D. J. Miller, Proc. of the ECFA workshop on LEP200, eds. A. Böhm and W. Hoogland, CERN 87-08, 202 (1987).
- [6] C. Peterson, P. M. Zerwas and T. F. Walsh, *Nucl. Phys.* **B229**, 301 (1983).
- [7] CELLO Collaboration, H.-J. Behrend et al., *Zeit. f. Phys.* **C43**, 1 (1989).
- [8] J. H. Field, proceedings of Photon '95, Sheffield U.K. 8-13 April 1995, eds. D. J. Miller, S. L. Cartwright and V. Khoze, World Scientific, Singapore, 490 (1995).
- [9] N. Arteaga et al., proceedings of Photon '95, Sheffield U.K. 8-13 April 1995, eds. D. J. Miller, S. L. Cartwright and V. Khoze, World Scientific, Singapore, 281 (1995).
- [10] N. Arteaga et al., *Phys. Rev.* **D52**, 4920 (1995);
N. Arteaga et al., *Phys. Rev.* **D53**, 2854 (1996).
- [11] P. Aurenche et al., Physics at LEP2, eds. G. Altarelli, T. Sjöstrand and F. Zwirner, CERN 96-01, 301 (1996).
- [12] M. Seymour, private communications.
- [13] OPAL Collaboration, K. Ahmet et al., *Nucl. Instr. and Meth.* **A305**, 275 (1991);
P. Allport et al., *Nucl. Instr. and Meth.* **A324**, 34 (1993);
P. Allport et al., *Nucl. Instr. and Meth.* **A346**, 476 (1994);
B. E. Anderson et al., *IEEE Transactions on Nuclear Science* **41**, 845 (1994).
- [14] J. A. M. Vermaseren, *Nucl. Phys.* **B229**, 347 (1983).
- [15] J. Allison et al., *Nucl. Instr. and Meth.* **A317**, 47 (1992); GEANT Detector Description and Simulation Tool, CERN Program Library Long Writeup W5013 (1993).
- [16] S. Jadach, B. F. L. Ward and Z. Was, *Comp. Phys. Comm.* **79**, 503 (1994).
- [17] G. Marchesini et al., *Comp. Phys. Comm.* **67**, 465 (1992).
- [18] S. J. Brodsky, T. Kinoshita and H. Terazawa, *Phys. Rev.* **D4**, 1532 (1971).
- [19] A. Buijs et al., *Comp. Phys. Comm.* **79**, 523 (1994).
- [20] G. D. Lafferty and T. R. Wyatt, *Nucl. Instr. and Meth.* **A355**, 541 (1995).

sources	background fraction	expected events
$e^+e^- \rightarrow Z^0 \rightarrow \tau^+\tau^-$	$(0.32 \pm 0.06)\%$	48 ± 9
$e^+e^- \rightarrow e^+e^-\tau^+\tau^-$	$(1.6 \pm 0.2)\%$	240 ± 30
$\gamma\gamma \rightarrow \text{hadrons}$	$(0.8 \pm 0.2)\%$	120 ± 30
Total	$(2.7 \pm 0.3)\%$	410 ± 40

Table 1: Expected background contributions.

cuts	$0.001 < x < 0.25$	$0.25 < x < 0.5$
statistics (data)	± 0.022	± 0.021
statistics (MC)	± 0.012	± 0.011
x resolution	± 0.002	± 0.004
Q^2 resolution	± 0.000	± 0.006
χ resolution	± 0.002	± 0.004
η resolution	± 0.004	± 0.001
y resolution	± 0.004	± 0.011
backgrounds	± 0.003	± 0.003
correction	± 0.008	± 0.008
$\frac{1}{2}\epsilon F_B^\gamma/F_2^\gamma$	$0.068 \pm 0.025 \pm 0.011$	$0.094 \pm 0.024 \pm 0.016$

cuts	$0.5 < x < 0.75$	$0.75 < x < 0.997$
statistics (data)	± 0.024	± 0.028
statistics (MC)	± 0.012	± 0.014
x resolution	± 0.003	± 0.014
Q^2 resolution	± 0.001	± 0.000
χ resolution	± 0.005	± 0.003
η resolution	± 0.003	± 0.003
y resolution	± 0.007	± 0.008
backgrounds	± 0.003	± 0.003
correction	± 0.006	± 0.009
$\frac{1}{2}\epsilon F_B^\gamma/F_2^\gamma$	$0.091 \pm 0.027 \pm 0.012$	$0.032 \pm 0.031 \pm 0.019$

Table 2: Contributions to the systematic error on $\frac{1}{2}\epsilon F_B^\gamma/F_2^\gamma$. The last row is the value obtained in each x range with its errors, the first being statistical and the second systematic.

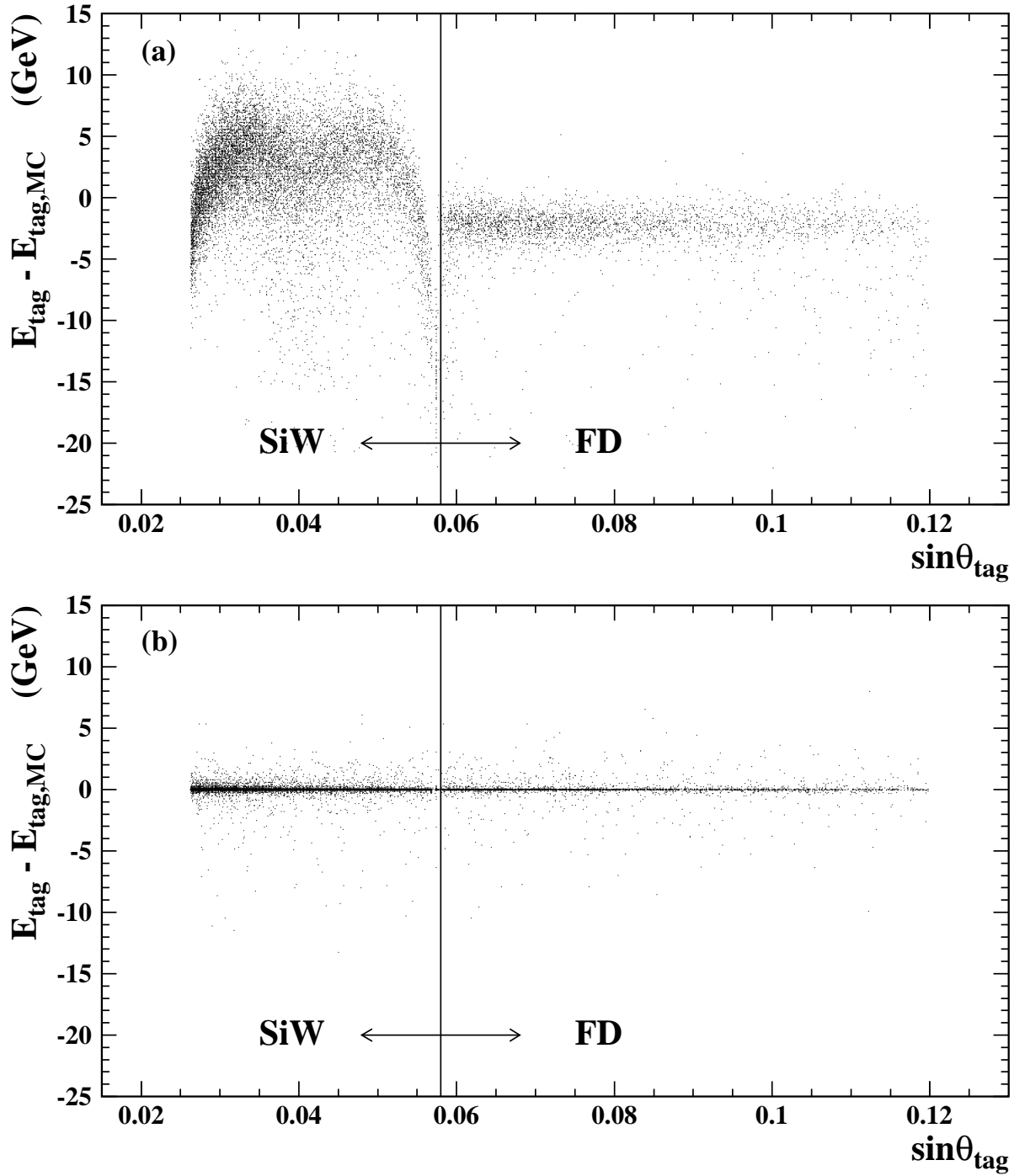


Figure 3: (a): $E_{\text{tag}} - E_{\text{tag,MC}}$ versus $\sin\theta_{\text{tag}}$ for E_{tag} measured directly by FD or SiW. (b): $E_{\text{tag}} - E_{\text{tag,MC}}$ versus $\sin\theta_{\text{tag}}$ for E_{tag} evaluated with the angle θ_{tag} measured by FD or SiW.

OPAL

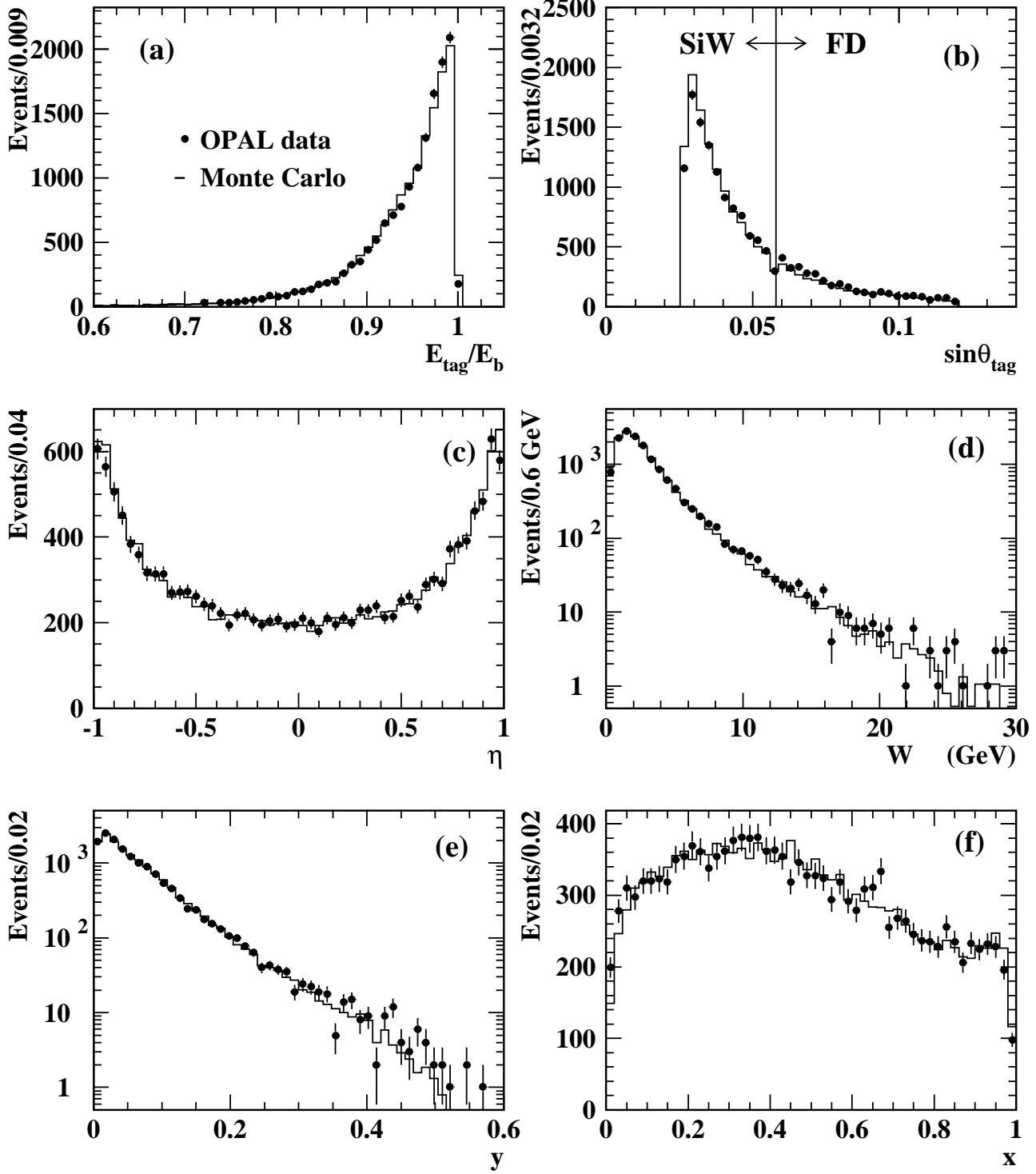


Figure 4: E_{tag}/E_b , $\sin\theta_{\text{tag}}$, η , W , y and x distributions for the data (points) compared to the Monte Carlo predictions (histograms).

OPAL

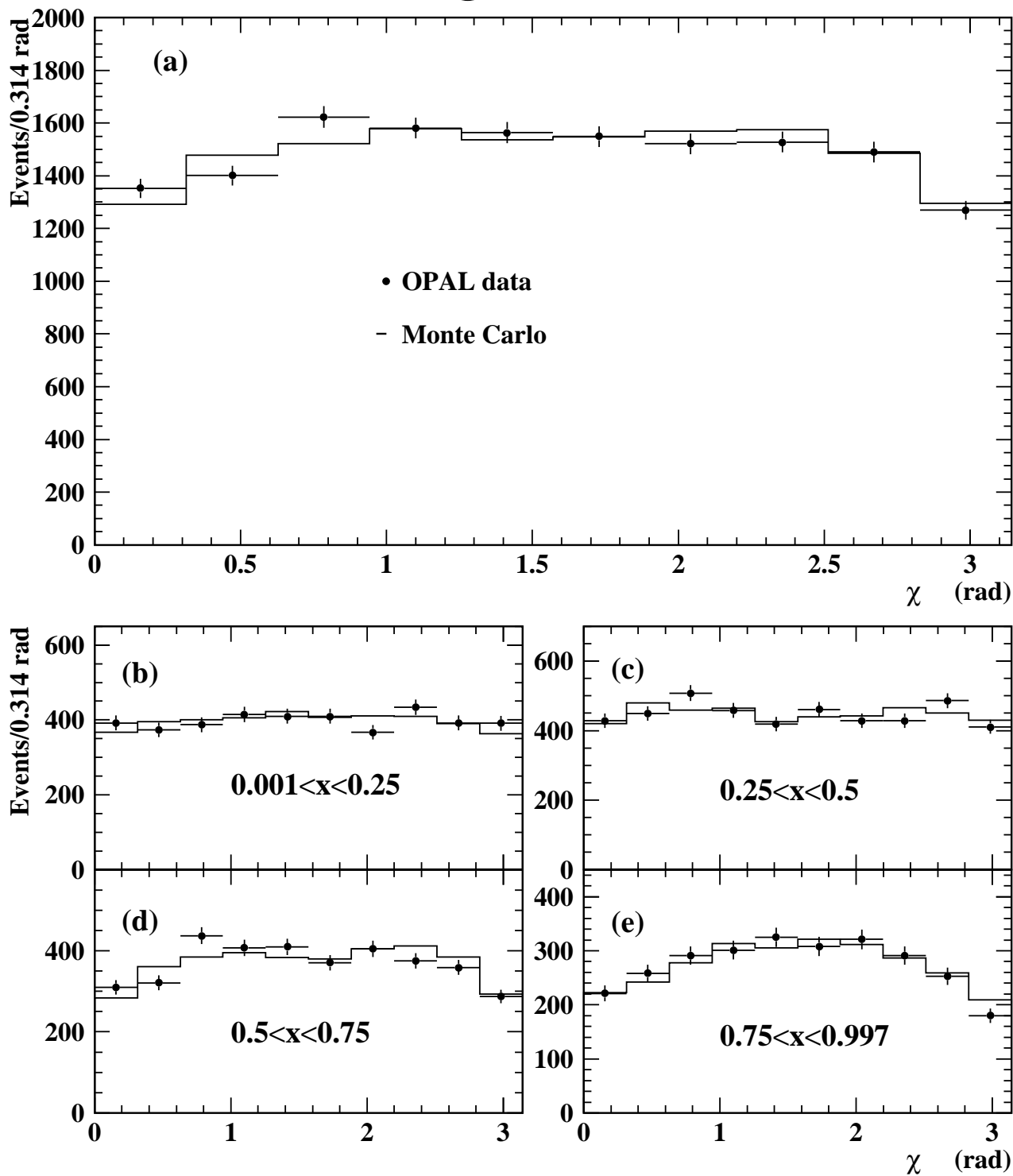


Figure 5: Azimuthal angle distributions for the whole x range (a) and for different ranges of x (b to e). The points represent the data and the histograms the Monte Carlo. The error bars are statistical only.

OPAL

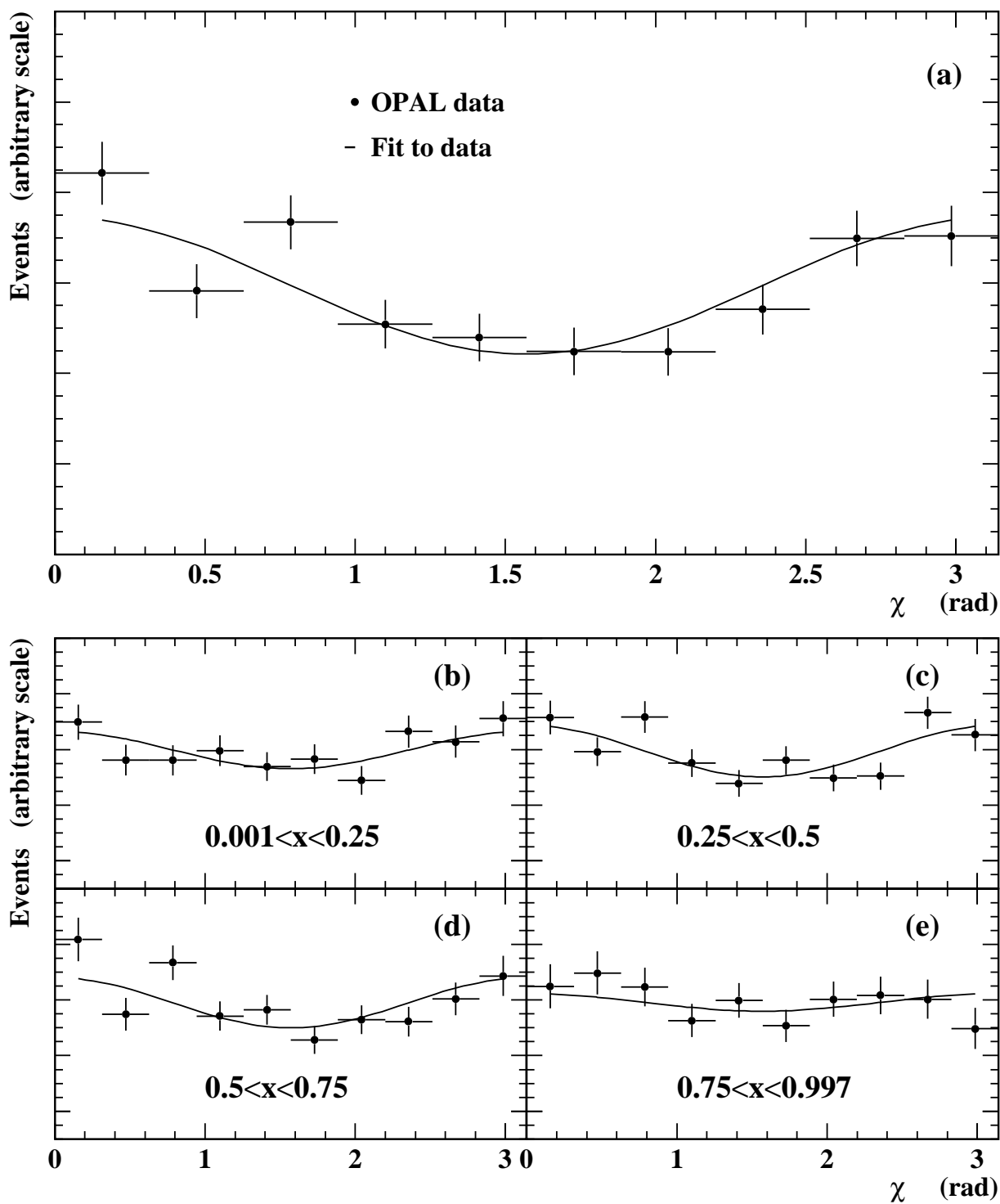


Figure 6: Corrected azimuthal angle distributions. The distributions were fitted with equation 13. The error bars are statistical only. In order to see clearly the variations of the fitted curve as a function of χ , the zero of the vertical scale has been suppressed.

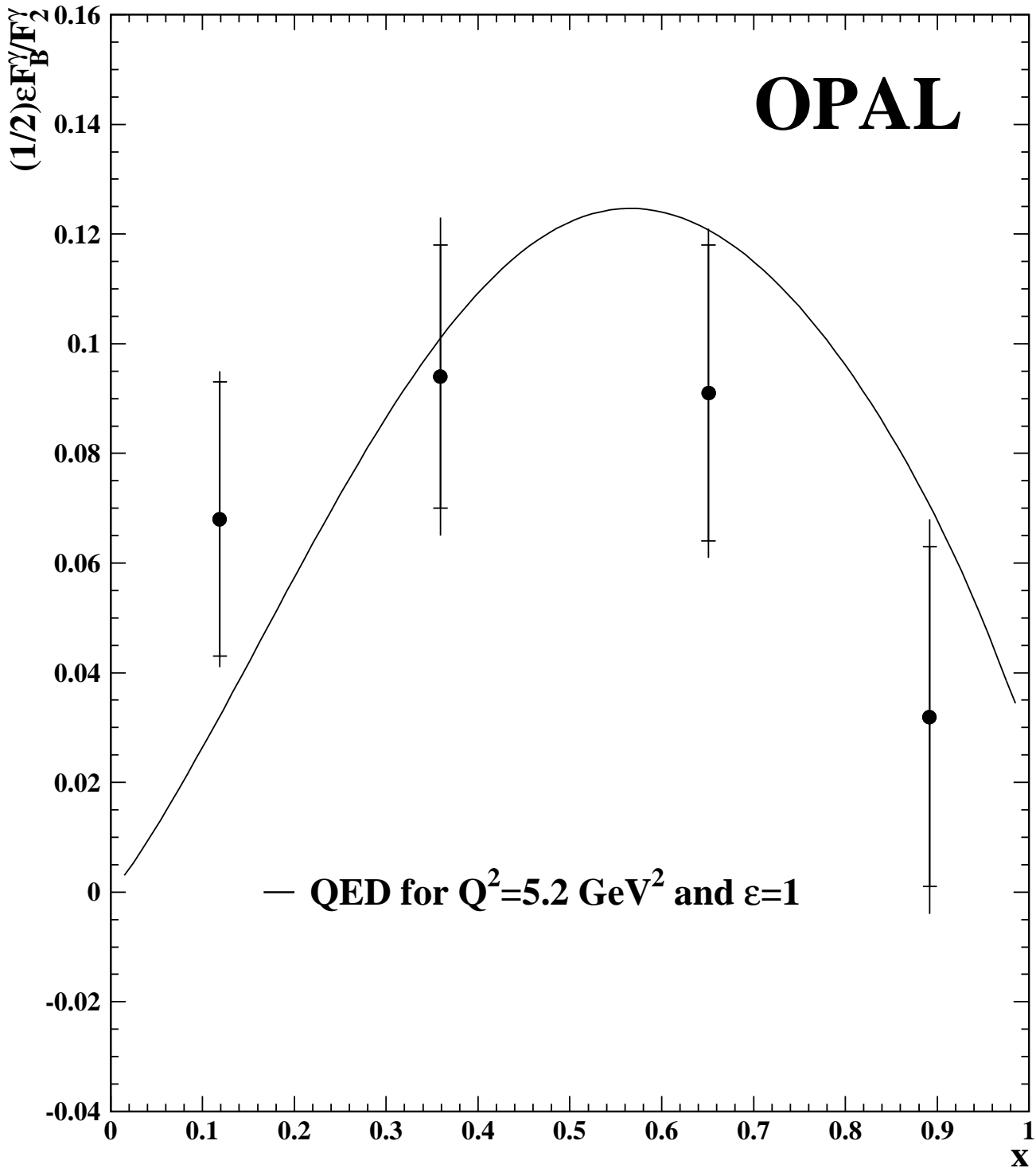


Figure 7: $\frac{1}{2}\epsilon F_B^\gamma/F_2^\gamma$ obtained from the azimuthal angle distributions corrected for the effects of the detector. The points are the data and the solid line is the QED prediction for $Q^2 = 5.2 \text{ GeV}^2$ and $\epsilon = 1$. The structure functions with their full mass dependence were used to plot the predicted ratio of F_B^γ to F_2^γ . The total (outer) error bars show the sum in quadrature of the statistical (inner error bars) and systematic errors.